Journal of Alloys and Compounds 747 (2018) 31–37

Contents lists available at ScienceDirect

Journal of Alloys and Compounds

journal homepage: http://www.elsevier.com/locate/jalcom

Kesterite Cu_2ZnSnS_4 thin films by drop-on-demand inkjet printing from molecular ink

Tapas K. Chaudhuri [a, *], Mitesh H. Patel [a], Devendra Tiwari [b], Prashant R. Ghediya [a]

[a] K. C. Patel Research and Development Centre, Charotar University of Science and Technology, Changa, Anand District, Gujarat 388421, India
[b] School of Chemistry, University of Bristol, Cantock's Close, Bristol, BS8 1TS, UK

ARTICLE INFO

Article history:
Received 25 October 2017
Received in revised form
1 March 2018
Accepted 3 March 2018

Keywords:
Copper tin zinc sulphide
Inkjet printing
Molecular ink
Thin film
Electrical properties

ABSTRACT

Inkjet printing of kesterite Cu_2ZnSnS_4 (CZTS) thin films on glass from molecular ink is described. CZTS ink consists of copper acetate, zinc acetate, tin chloride and thiourea dissolved in a mixture of ethylene glycol and isopropyl alcohol. The printed precursor films are vacuum dried and thermolysed at 200 °C in air to obtain CZTS films. X-ray diffraction and Raman spectroscopy of films confirm the formation of kesterite CZTS without any secondary phases. The band gap of the films is 1.48 eV as deduced from transmission spectrum using Tauc plot. The films are p-type with hole density and mobility of 2.65×10^{19} cm^{-3} and 0.3 $cm^2V^{-1}s^{-1}$, respectively. Measurement of electrical conductivity of films in the temperature range from 77 to 300 K show that dominant mechanisms of conduction are Mott-Variable Range Hopping, Nearest Neighbour Hopping and Thermally Activated Band Conduction in the temperature ranges of 77–155 K, 180–240 K and 250–300 K, respectively.

1. Introduction

Inkjet printing (IJP) is a direct-write, non-contact, non-vacuum and atmospheric method for deposition of solid thin films [1]. In this technique, picolitre drops of a liquid ink are impelled onto a substrate to precisely deposit films in pre-defined pattern. The ejected drops fall until they come in contact with the substrate. The drops spread because of momentum and surface tension and eventually coalesce on the substrate to form a film. Printed solid film is then formed by solvent evaporation. IJP has high material utilization factor. Printing of films can be sequential or layer-by-layer and can form any pattern without masks. Printed films are likely to be contamination free because of non-contact deposition. Further, IJP is amenable to large scale roll-to-roll deposition of films. Printing of films on a substrate depends on inkjet ink, jetting voltage and dots per inch (DPI). IJP has been utilized for fabrication of variety of devices and films, such as, flexible electronics [2–4], organic electronics [2,3,5], metal electrical contacts [3,4,6], photo-detectors [5,7,8], sensors [9–11], optoelectronic devices [7], thermoelectric devices [12], supercapacitors [13], micro-batteries [14], smart windows [15], ceramics [16], organic solar cells [17–19] and perovskite solar cells [18].

The special attributes of IJP have not been fully exploited for inorganic solar cells and only few investigations [20–26] have been reported so far. There are some recent studies on inkjet-printed $Cu_2ZnSn(S,Se)_4$ (CZTSSe) solar cells [20,25,26], Cu_2ZnSnS_4 (CZTS) films [21] In_2S_3 non-toxic buffer layers [22], $Cu(In,Ga)(S,Se)_2$ (CIGSSe) solar cells [23] and NiO dye-sensitized solar cells [24]. Lin et al. [20] were first to demonstrate inkjet-printing of solar cells. Solar cells with Mo/CZTSSe/CdS/i-ZnO/ZnO:Al/Ni:Al grids were fabricated based on the inkjet-printed CZTSSe absorbers. CZTS precursor layers were IJP on Mo/glass substrates from CZTS ink. Molecular solution ink was prepared by dissolving copper (II) chloride, zinc acetate dihydrate, tin (II) chloride dihydrate, thiourea and sodium fluoride in dimethyl sulfoxide (DMSO) with the help of overnight stirring. The printed precursor layers were preheated at 300 °C in air for 2 min to remove solvent. Later, the films were finally annealed in Se vapour at 560 °C for 20 min to obtain large-grained CZTSSe films. CZTSSe solar cell with an active area of 0.5 cm^2 yielded power conversion efficiency of 6.4% with an open circuit voltage (V_{OC}) of 431 mV, short current density (J_{SC}) of 34.6 mA/cm^2 and fill factor (FF) of 42.8%, respectively.

Colina et al. [25] optimized the inkjet-printed precursor films for CZTSSe solar cells. Light-yellow coloured CZTS molecular ink was made by stirring overnight DMSO containing copper (II) acetate monohydrate, tin (II) chloride dehydrate and anhydrous zinc (II)

* Corresponding author.
E-mail address: tkchaudhuri.rnd@gmail.com (T.K. Chaudhuri).

https://doi.org/10.1016/j.jallcom.2018.03.028
0925-8388/

chloride. The precursor films were printed layer-by-layer on Mo-coated glass and dried at different temperatures (180°, 220° and 280° C) in air. The dried precursor films were then converted to CZTSSe absorbers by annealing in Se vapour at 550 °C for 45 min. Higher drying temperatures of precursor helped in grain growth and recrystallization of CZTSSe films. Solar cells with architecture of Mo/$MoSe_2$/CZTSSe/CdS/i-ZnO/ITO were fabricated and performances were optimized with respect to drying temperature and number of printed precursor layers. The best solar cell was obtained for drying temperature of 280 °C and 5 layer printing (1.9 μm). The solar cell (without any antireflection coating) showed photo-conversion efficiency was 6.55% with V_{OC}, J_{SC} and FF as 366 mV, 33 mA/cm^2 and 54%, respectively.

In continuation of their earlier work [20] on IJP CZTSSe solar cells, Lin et al. [26] also studied the effect of sodium (Na) in inkjet-printed CZTSSe absorber on solar cell performance. Sodium is known to have a positive effect on the morphology as well as electronic properties of CZTSSe absorbers. Incorporation of sodium in CZTSSe results in improved grain growth, increase of charge carrier concentration and/or mobility, passivation of deep defects, increase of open-circuit voltage (V_{OC}) and fill factor and conversion efficiency. For Na doping in printed CZTSSe films, different concentrations of NaF were added in the CZTS molecular ink. It was found that 0.144 M NaF produced the best CZTSSe solar cell with conversion efficiency of 6.4%.

Both Lin et al. [20] and Colina et al. [26] have printed CZTS films from molecular solution inks. In a different approach, Martini et al. [25] have inkjet-printed CZTS films from nanoparticle ink. CZTS nanoparticles of 3–5 nm sizes were continuously synthesized from an aqueous solution of tin (IV) chloride, copper acetate monohydrate, zinc acetate dihydrate, 3-mercapto acetic acid and sodium sulphide in a microwave reactor. Nanoparticles were washed, centrifuged and then redispersed in methyl-ethyl-ketone with 10% (v/v) of 1-dodecan-thiol to form inkjet ink. The ink was then used for printing of CZTS films with an inkjet material printer. The as-printed films were dried for 1 h under vacuum at 190 °C and then at 300 °C. The ultimate CZTS films with large grains were obtained by annealing in sulphur vapours at 540 °C for 3 h.

IJP was utilized for developing In_2S_3 films [22] as non-toxic Cd-free buffer layer for CIGSSe thin film solar cells. Precursor ink consisted of indium nitrate and thiourea dissolved in ethanol with 10% (v/v) ethylene glycol. The performances of CIGSSe solar cells with conventional CdS and In_2S_3 buffer layers were at par with efficiencies above 12%. Lin et al. [23] reported inkjet-printed CIGSSe solar cells with 12.3% conversion efficiency. Precursor Cu–In–Ga molecular ink was prepared from by mixing the metal nitrate precursors in a solvent mixture of 2-propanol and ethylene glycol. The printed precursor layers on Mo-coated glass were dried at 250 °C for 2 min in air. The dry precursor films were then selenized and sulfurized at 400° to 580 °C to obtain the desired CIGSSe films. Inkjet-printed solar cell of 0.5 cm^2 area achieved an efficiency of 11.3% with V_{OC}, J_{SC} and FF of 541 mV, 31.1 mA/cm^2 and 67.0%, respectively. Preliminary assessment on utilization of inkjet-printed p-type NiO films for dye-sensitized solar cells was carried out by Brisse et al. [24] and concluded that IJP is promising.

In this paper we report inkjet printing of CZTS films on glass from a simple molecular solution ink. The ink consists of a solution of (Cu^{+}-Zn^{+2}-Sn^{+2})-thiourea (CZTTU) complex dissolved in a blend of ethylene glycol and isopropanol which can be easily prepared in 10 min. The printed precursor films were first dried at 70 °C in vacuum followed by heating in air at 200 °C. Films thus obtained are kesterite CZTS as confirmed by X-ray diffraction and Raman spectroscopy. Electrical properties of such films have been also investigated in the wide temperature range of 77–300 K.

2. Experimental

2.1. Formulation of ink

Molecular solution ink basically consists of a precursor dissolved in an appropriate solvent. Chaudhuri and Tiwari [27] showed that precursor of (Cu^{+}-Zn^{+2}-Sn^{+2})-thiourea (CZTTU) complex yields kesterite CZTS on heating at 200 °C in air. Precursor solution ink was prepared by dissolving copper (II) acetate monohydrate (0.1 M), zinc acetate dihydrate (0.05 M), tin (II) chloride (0.05 M) and thiourea (TU, 0.5 M) in methanol. CZTS films were deposited on glass by dip-coating and subsequently heating the precursor films at 200 °C in air. Later, Ghediya et al. [28] also reported doctor-blade coating of CZTS films from a solution of CZTTU complex in ethylene glycol (EG). Hence, CZTTU complex was chosen as the precursor for CZTS films.

Next step was to select appropriate solvent suitable for inkjet printing. The solvent had to satisfy the following criteria: (i) It should dissolve readily all the precursor chemicals mentioned above, (ii) Viscosity should be between 10 and 12 cPs, (iii) Surface tension should be between 28 and 33 dyn/cm and (iv) Boiling point should be as low as possible. As mentioned above, the precursor chemicals readily dissolved in both methanol [27] and EG Ref. [28]. Hence, a mixture of EG and isopropanol (IP) was used as the solvent. EG-IP mixtures with different proportions were prepared and viscosity and surface tension were measured to tune the fluid properties to the desired values. It was found that a blend of 40% by volume of EG with 60% by volume of IP has viscosity and surface tension of 10 cPs and 35 dyn/cm, respectively which was close to the targeted values. Thus, for preparing inkjet printing ink, solvent with 40% EG and 60% IP was used. Inkjet ink was prepared by dissolving copper (II) acetate monohydrate (0.2 M), zinc acetate dihydrate (0.1 M), tin (II) chloride (0.1 M) and thiourea (0.8 M) in EG-IP at room temperature (~300 K). At first, 50 mL of EG-IP was taken in a beaker and stirred continuously by a magnetic stirrer. Copper (II) acetate powder was slowly added to EG. A dark blue suspension was formed which turns into dark blue clear solution on adding a few drops of concentrated hydrochloric acid. Then zinc acetate powder was slowly put into the solution which gradually changes into light green colour. Further addition of tin (II) chloride turns the solution into light yellow. Finally, thiourea (TU) powder was slowly introduced into the solution which first becomes curdy and then turns colourless as shown in Fig. 1. TU reduces Cu(II) to Cu(I) under acidic condition to form colourless $[Cu(TU)3]^{+}$ complex [29]. TU also forms complexes with Zn^{++} and Sn^{++} as $[Zn(TU)_2]_{++}$ and $[Sn(TU)]^{++}$, respectively. Finally, a colourless complex $[CuZnSn(TU)_n]^{m+}$ is formed in the EG-IP solvent which is the desired CZTS molecular solution ink. Total time taken for preparing CZTS ink is about 10 min. The ink has been found to be very stable

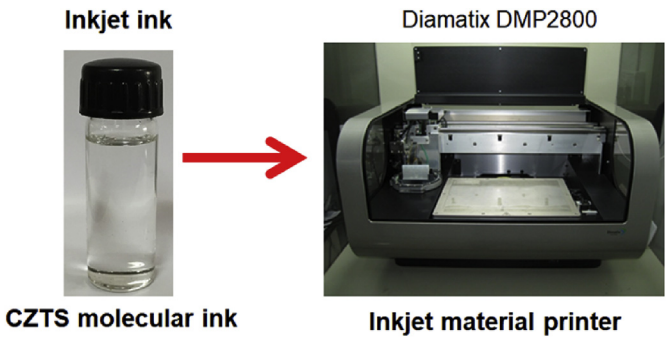

Fig. 1. Colourless CZTS molecular ink prepared for inkjet material printing.

for more than a year. Here, EG not only acts as a solvent but also as stabiliser for transparent ink. All the chemicals and solvents used in present study are of Analytical Grade supplied by Merck Limited, India.

2.2. Printing of films

The precursor films were printed on glass substrates using an Inkjet Material Printer (DMP2800, Fujifilm Dimatix Inc.). The molecular ink was filtered with a 200 nm filter and injected into a Dimatix printing cartridge (DMC-11610). Scrupulously cleaned glass substrates of sizes 75 mm × 25 mm X 2 and 75 mm × 75 × 2 mm were used for printing. Precursor films of 20 mm × 10 mm patches were printed on the substrates. The printing head has piezo-driven jetting devices with 16 nozzles at 256 μm spacing, each capable of producing drops of 10 pL. The distance between the substrates and printer head was fixed at 1.3 mm. The jetting voltage and dots per inch (DPI) was adjusted to 24 V and 1411, respectively. The films were first dried at 70 °C in vacuum oven (EQ-DZF-6050, MTI Corp.) under a vacuum of 2 torr for 30 min. The solid precursor films were then heated in an oven at 200 °C for 20 min in air for thermolysis to shiny brown CZTS films. Hence, inkjet printing of CZTS films consisted of 3 steps: Inkjet printing of wet precursor films, vacuum drying of prints to get solid precursor films and finally thermolysing the precursor films to CZTS films by heating at 200 °C in air. In the present study, CZTS films were not subjected any further heat treatment or annealing. Thickness of a single printed film was around 150 nm. For obtaining higher thickness, CZTS films can be printed sequentially one on top of another.

2.3. Characterizations

The composition and crystalline nature of the films were studied by X-ray Diffractometer (Bruker, D2 PHASER). XRD plots were recorded in the 2Θ range from 10° to 70° with Ni-filtered CuK_α radiation. The transmittance spectra of the films were measured with a UV–Vis-NIR Spectrophotometer (Shimadzu, UV-3600) in the wavelength range of 300–2400 nm. Cross-sectional views of films were observed by Scanning Electron Microscope (SEM, LEO S-440i) with Energy Dispersive Spectroscopy (EDS). The thickness of the films was also estimated from cross-sectional SEM. The vibrational modes of CZTS were studied by Raman Spectrometer (Jobin–Yvon, HR800) with an excitation wavelength of 514 nm. A linearly polarized Ar-ion laser beam with a power of 10 mW was focused into a spot size of 1 μm diameter.

For electrical measurements gap cells (~2 mm) were made with graphite paint (Ted Pella) as ohmic contacts. The type of conduction in the films was determined by hot probe method. The electrical conductivity was measured in the temperature ranges of 77–300 K by placing the samples in an optical cryostat (Janis VPF-100). The dark current was measured and recorded with a Source/Meter Unit (Keithly 2611) with a DAQ card. During measurements, a constant voltage of 10 V was applied across the contacts of the samples.

3. Results and discussion

The CZTS molecular ink synthesized in the present study was colourless and transparent as shown in Fig. 1 and took about 10 min to prepare. The stable ink was prepared by dissolving precursor chemicals in a mixture of EG-IPA by stirring. Earlier, Lin et al. [20] and Colina et al. [26] also prepared molecular ink for IJP of CZTS films. In both cases, CZTS inks were made by dissolving precursor chemicals in DMSO by stirring overnight (~15 h). The preparation time of molecular ink suggested in the present study is reduced drastically from about 15 h to 10 min.

3.1. Inkjet-printed films and characterizations

Fig. 2 shows the inkjet-printed CZTS films on glass substrate. Some dots can be found on the final films. This may arise during heating. The films are made up of only a single precursor layer resulting in thickness of 150 nm. Higher thickness can be achieved using layer-by-layer deposition. Chaudhuri and Tiwari [27] showed that single precursor layer of CZTS prepared in methanol resulted in 90 nm. However, it was found that same precursor in EG gives higher thickness because of higher concentration of chemicals.

X-ray diffractogram (XRD) of a typical inkjet-printed CZTS film is shown in Fig. 3. There are lines superimposed on background hump because of glass substrate. The XRD lines are identified to be of kesterite CZTS (JCPDS File 26-0575) only due to reflections from (112), (200) and (312) planes. The lines are also broad suggesting that the films are nanocrystalline. The average crystallite size deduced from the Scherrer relation is found to be ~10 nm. Similar results were reported by Chaudhuri and Tiwari [27] for the CZTS films prepared from methanolic ink.

Theoretical and experimental results showed that thermodynamic equilibrium single-phase CZTS is expected to exist only in a narrow region of the pseudo-ternary Cu_2S-ZnS-SnS_2 phase diagram. The narrow phase stability makes defects and secondary phase easy to form during the deposition processes. A slight deviation from the optimal growth conditions (1–2%) will result in the formation of secondary phases, including, ZnS, Cu_2SnS_3 (CTS), SnS, SnS_2 and CuS. Hence, to confirm the stoichiometry of CZTS, Energy Dispersive Spectroscopy (EDS) was performed. EDS results of printed CZTS films show the presence of Cu, Zn, Sn, S as the major elements. The [Cu]/([Zn]+[Sn]) and [Zn]/[Sn] ratios are found to be 0.83 and 1.12, respectively, revealing Cu-poor and Zn-rich stoichiometry [20,21,28]. CZTS solar cells with such compositions have yielded the best efficiency.

There are no extra XRD lines (Fig. 3) due to any secondary phases, such as, ZnS, Cu_2S, Cu_2SnS_3 (CTS), etc. However, crystal structure of CZTS, CTS and ZnS are identical and hence they cannot be detected by XRD alone. Hence, Raman spectroscopy is required to confirm the pure phase. Fig. 4 shows the Raman shift spectrum of an inkjet-printed CZTS thin film whose XRD is presented in Fig. 3. The spectrum shows the signature peak at 340 cm^{-1} for kesterite CZTS. There are no other secondary lines due to CuS, ZnS, SnS or Cu_2SnS_3. The peak at 340 cm^{-1} is due to the A1 vibrational mode, arising from the vibrations of sulphur atoms in CZTS lattice while rest of the atoms remains stationary [30]. Thus, it is confirmed that inkjet printing from molecular ink (Fig. 1) synthesized in the present study produce pure CZTS films.

The bandgap of printed CZTS film was determined from transmittance spectrum measured in the wavelength range of 350–2400 nm. Fig. 5 (a) shows the transmittance spectrum of single layer deposited CZTS thin film. It can be seen from the Fig. that the transmittance of the film decreases rapidly below 1000 nm due to absorption by CZTS.

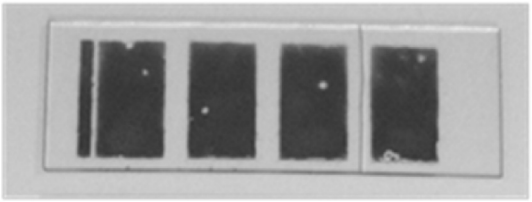

Fig. 2. Inkjet-printed CZTS thin films on glass.

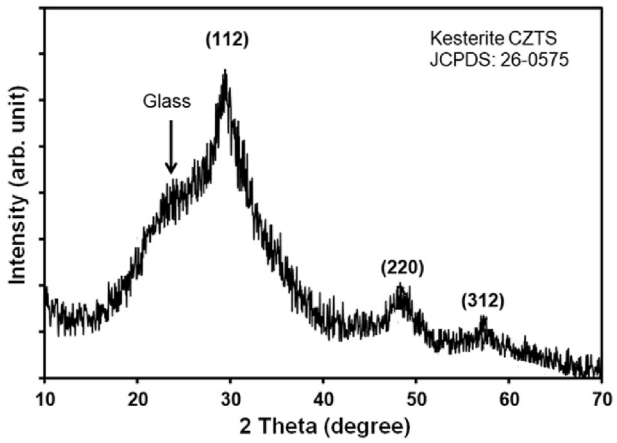

Fig. 3. X-ray diffractogram of inkjet-printed CZTS film on glass.

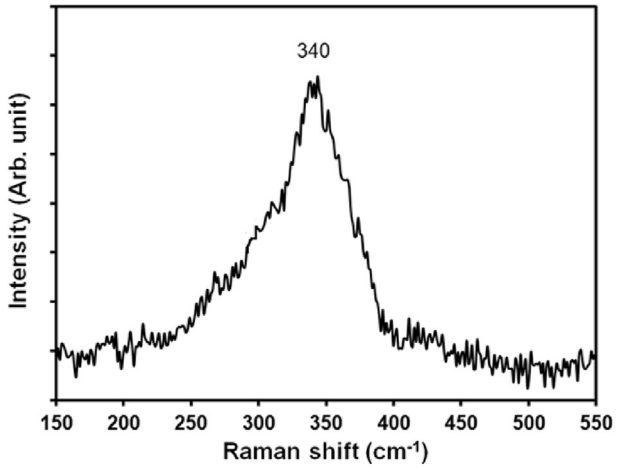

Fig. 4. Raman spectrum of inkjet-printed CZTS thin film indicating kesterite phase.

The transmittance data was used to calculate the absorption coefficient (α) using Eq. (1):

$$\alpha = \frac{1}{d} \ln \frac{1}{T} \quad (1)$$

where,

d is the thickness and
T is the transmittance of the film

Band gap of CZTS film is determined from the Tauc relation [31] for direct band gap semiconductors:

$$\alpha h\nu = A(h\nu - Eg)^{1/2} \quad (2)$$

where,

α is the absorption coefficient
h is Plank's constant
ν is the frequency of radiation
A is an appropriate constant
E_g is the band gap (eV)

Fig. 5(b) shows the Tauc plot of $(\alpha h\nu)^2$ Vs. hν for printed CZTS film. The band gap of the CZTS film was deduced by extrapolating linear portion of the plot to zero and found to be 1.48 eV. This is in good agreement with the reported [32] value of 1.5 eV for bulk CZTS.

The cross-section of a CZTS thin film as viewed by SEM is presented in Fig. 6 which reveals that the film is smooth and homogeneous. The existence of porosity has not been observed. This is similar to the CZTS films made from methanolic solution of CZTTU complex [27]. The above results indicate that IJP precursor films yield CZTS film at 200 °C. IJP ink is a molecular solution of CZTTU complex in EG-IP. This is considerably lower than the temperatures reported by Lin et al. [20] and Colina et al. [25]. Precursor films printed by Lin et al. [20] were first pre-heated at 300 °C for solvent removal and then heated at 560 °C in Se. Colin et al. [25] also dried the printed precursor films at 280 °C before selenizing at 550 °C. Further, synthesis of molecular ink by Lin et al. [20] and Colina et al. [25] takes quite long time: overnight soaking of the precursor chemicals in DMSO. In the present investigation preparation of ink takes only 10 min.

3.2. Electrical properties

Printed CZTS film was p-type with electrical conductivity (σ) and thermoelectric power (TEP) of 0.5 S/cm and +100 μV/K, respectively. The hole concentration (p) and mobility (μ) of the film was 2.65×10^{19} cm^{-3} and 0.3 $cm^2V^{-1}s^{-1}$, respectively as deduced

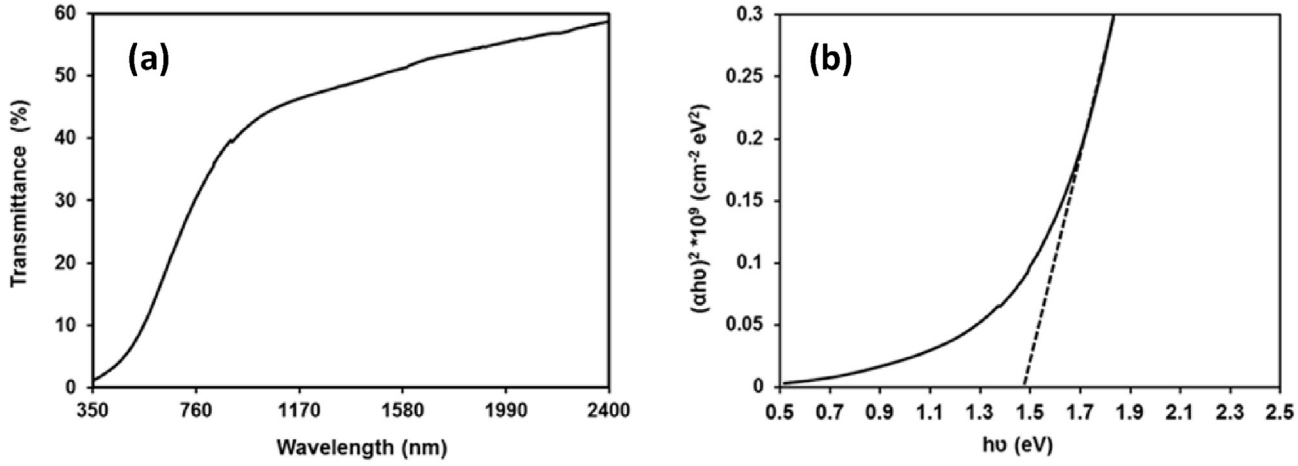

Fig. 5. (a) Transmittance spectrum of inkjet-printed CZTS film showing absorption edge and (b) Tauc plot of film indicating direct bandgap of 1.48 eV.

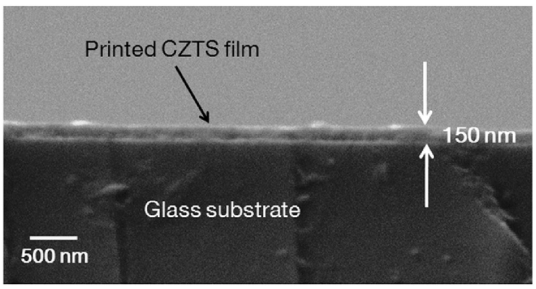

Fig. 6. Scanning electron micrograph of the cross-section of a CZTS film inkjet-printed on glass.

from TEP and σ. This high value of *p* is probably due to impurities in precursor chemicals and defects. Similar values were also observed for CZTS films dip-coated [27] and doctor-bladed [28] from molecular inks made from same precursor chemicals.

The temperature variation of electrical conductivity (TVEC) of a typical printed CZTS film from 77 to 300 K is shown in Fig. 7 as represented by the plot of ln(σ) vs. 1/T. In general, the conductivity of film increases with increase in temperature which is characteristic behaviour of a typical semiconductor film. At low temperatures below 125 K (until 77 K), conductivity of the film almost remain constant with temperature. However at higher temperatures above 200 K, the conductivity of the film increases rapidly. The distinctive features of TVEC of a sample depends on the modes of conduction dominant. It has been found that different types of electronic conduction processes [28,33,34] take place in CZTS films depending on the temperature range. These include, Efros–Shklovskii variable range hopping (ES-VRH), Mott variable range hopping (M-VRH), nearest neighbour hopping (NNH), thermionic emission over grain boundary barriers (TE over GBB) and thermally activated band conduction (TABC).

In general, hopping conduction in samples occurs below about 180 K through defect states in the band gap. Above about 180 K, polycrystalline CZTS samples show band conduction due to TE over GBB or TABC from defect states. Hence, the data of Fig. 7 was fitted with different models to identify the modes of conduction prevalent in the printed CZTS film.

In the temperature region of 77–155 K, the plot of $\ln(\sigma)\sqrt{T}$ Vs. $T^{-0.25}$ was linear as shown in Fig. 8 which implies that conduction is due to M-VRH. The temperature variation of conductivity of sample under M-VRH is given by

$$\sigma\sqrt{T} = \sigma_{0M}\, exp\left(\left(-\frac{T_M}{T}\right)^{\frac{1}{4}}\right) \tag{3}$$

where,

σ_{0M} is the hopping conductivity
T_M is Mott characteristics temperature
T is the temperature

The Hopping Energy calculated from the slope of the Eq. (3) is found to be 5 meV. This value is less than 10 meV and $T_o/T \gg 1$ which confirms M-VRH conduction at low temperatures in these CZTS films. Similar results were reported earlier [34–37]. Guo et al. [35] have observed that sol-gel derived CZTS films show M-VRH conduction in the temperature range of 40–175 K. Conduction by M-VRH from 70 to 170 K was also observed by Anasari et al. [34] for CZTS films prepared by ultrasonic assisted chemical vapour deposition. Hamdi et al. [36] reported M-VRH conduction from 80 to 160 K in CZTS pellets. Ghediya et al. [37] also noticed that conductivity of dip-coated CZTS film in the range 77–150 K is because of M-VRH.

In the temperature range of 180–240 K, the plot of ln(σ) Vs. 1/T, representing conduction by NNH, was found to be linear as shown in Fig. 9. The variation of conductivity with temperature of samples by NNH is given by

$$\sigma = \sigma_0 \exp\left(-\frac{E_{NNH}}{K_b T}\right) \tag{4}$$

where,

σ_0 is an appropriate constant
E_{NNH} is the hopping energy
k_b is the Boltzmann constant
T is the temperature

Hence, the conduction of printed CZTS films is dominated by NNH in the temperature range of 180–240 K. The Hopping Energy

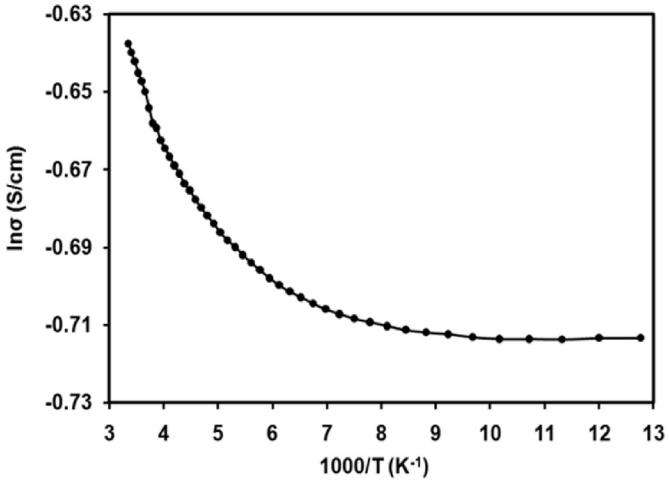

Fig. 7. Temperature variation of electrical conductivity of an inkjet-printed CZTS film in the temperature range from 77 to 300 K.

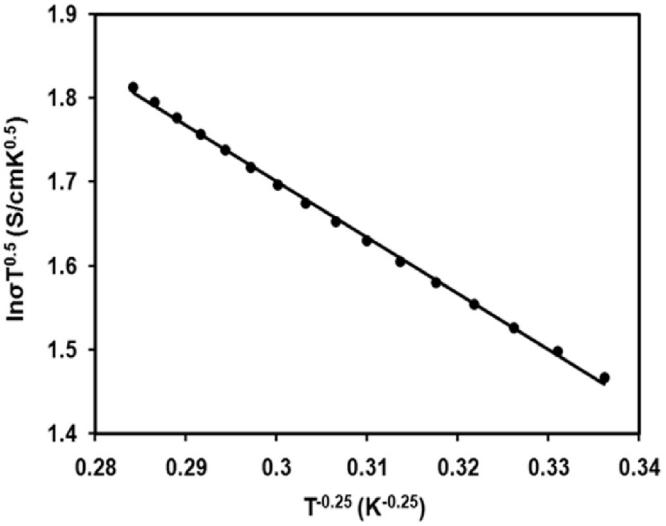

Fig. 8. Plot of $\ln(\sigma)\sqrt{T}$ vs. $T^{-0.25}$ for inkjet-printed CZTS film indicating Mott-Variable Range Hopping in the temperature range of 77–155 K.

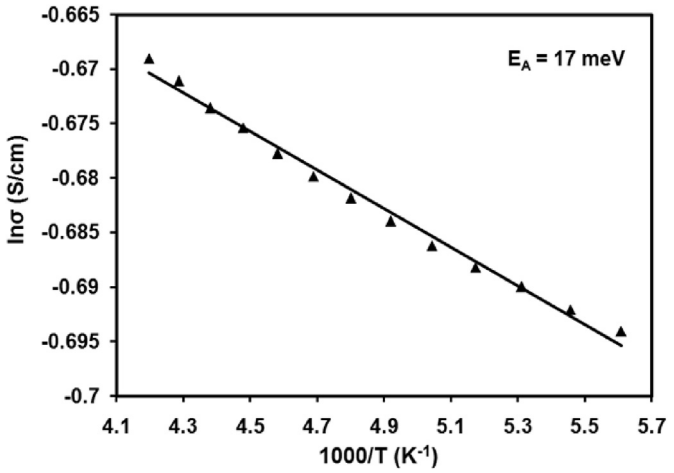

Fig. 9. Plot of ln(σ) vs. 1/T for inkjet-printed CZTS film suggesting Nearest Neighbour Hopping in the temperature range of 180–240 K.

is deduced to be 17 meV. This in agreement with the results of Ansari et al. [34] who also observed NNH conduction in CZTS films in the temperature range of 170–250 K with hopping energy of about 20–30 meV.

Finally, analysis of the conductivity data in the temperature range 250–300 K show that the plot of ln(σ) Vs. 1/T is linear as shown in Fig. 10. This reveals that conductivity is thermally activated given by the equation:

$$\sigma = \sigma_0 \exp\left(-\frac{E_a}{K_b T}\right) \quad (5)$$

where,

σ_0 is a constant and
E_a is activation energy
k_b is the Boltzmann constant
T is the temperature

Thus, electrical conduction in printed CZTS film is due to thermally activated band conduction in the temperature range of 250–300 K. The activation energy deduced from slope of the plot is

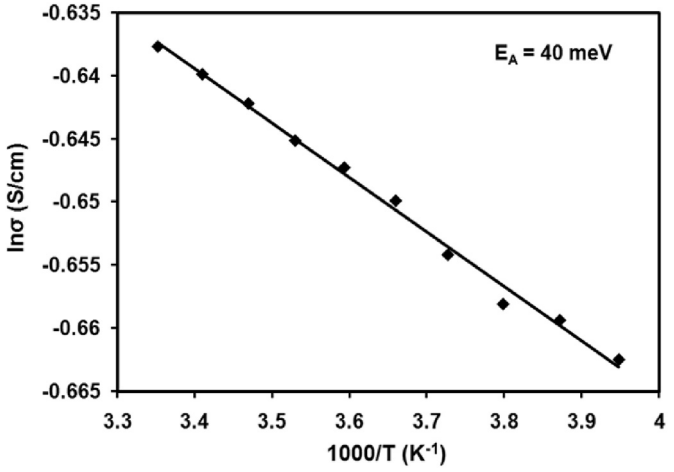

Fig. 10. Plot of ln(σ) vs. 1/T for inkjet-printed CZTS film in the temperature range of 250–300 K.

40 meV. This is probably due to thermal release of holes from defect states copper vacancies (V_{Cu}) situated at 20 meV above valence band and clusters. Furthermore, It can be seen that ln(σ) vs. 1/T plot can be fitted with two straight lines: one at higher temperature range (>200 K) and the other at lower temperatures range (<200 K), which indicates the presence of NNH conduction in the lower temperature range. A significant change in activation energy at both the temperature also suggests existing of different transport mode at different temperature.

The temperature variation of conductivity (Fig. 7) of inkjet-printed CZTS films can be expressed as

$$\sigma = \frac{\sigma_{0M}}{\sqrt{T}} \exp\left(\left(-\frac{T_M}{T}\right)^{\frac{1}{4}}\right) + \sigma_{0N} \exp\left(-\frac{E_{NNH}}{K_b T}\right) + \sigma_0 \exp\left(-\frac{E_a}{K_b T}\right) \quad (6)$$

The first term of the expression is conduction due to M-VRH prevalent from 77 to 155 K; the second term signifies NNH conduction predominant from 180 to 240 K and third term denotes thermally activated band conduction dominant from 250 to 300 K.

The inkjet-printed CZTS films in the present investigation are basically nanocrystalline. The films are p-type with hole concentration of ~10^{19} cm^{-3}. These films will have dominating intrinsic defects, such as, copper vacancies, V_{Cu} (at 20 meV) and copper on zinc antisites, Cu_{Zn} (120 meV) acting as acceptor levels. High hole concentration in these films implies that density of defect states (situated near the valance band) are also high. Hence, conduction of holes by hopping through these defects states is highly probable. When a printed CZTS film is at low temperatures (<250 K), the most of the holes are in the acceptor levels. The thermal energy at these temperatures is insufficient to push the holes to the valence band for conduction. But the energy is sufficient to allow hopping from one level to another in the acceptor levels.

4. Conclusions

Kesterite CZTS films can be inkjet printed on glass from molecular ink consisting of (Cu^{+}-Zn^{+2}-Sn^{+2})-thiourea complex dissolved in ethylene glycol and isopropanol mixture. The formation of kesterite CZTS were confirmed by XRD and Raman spectroscopy. No other secondary phases were detected. The band gap of inkjet-printed CZTS films is 1.49 eV. The films are p-type with conductivity, hole concentration and mobility of 0.5 S/cm, 2.65 × 10^{19} cm^{-3} and 0.3 $cm^2V^{-1}s^{-1}$, respectively. Analysis of temperature dependence electrical conductivity of CZTS films reveals hopping conduction and thermally activated band conduction at lower and higher temperatures, respectively.

Acknowledgements

This work was funded by a grant (DST/TM/SERI/2K10/25) from the Department of Science and Technology, Government of India. The authors are also thankful to Dr. Abhijit Ray, Department of Solar Energy of Pundit Deendayal Petroleum University, Gandhinagar for ungrudging help during this work.

References

[1] S.D. Hoath (Ed.), Fundamentals of Inkjet Printing: the Science of Inkjet and Droplets, Wiley-VCH Verlag, Weinheim, 2016.
[2] Y.Z. Ping, H.Y. An, B.N. Bin, W.X. Mei, X.Y. Lun, Inkjet printing for flexible electronics: materials, processes and equipments, Chinese Sci. Bull. 55 (2010) 3383–3407.
[3] M. Gao, L. Li, Y. Song, Inkjet printing wearable electronic devices, J. Mater. Chem. C 5 (2017) 2971–2993.
[4] N.C. Raut, K. Al-Shamery, Inkjet printing metals on flexible materials for plastic and paper electronics, J. Mater. Chem. C 6 (2018) 1618–1641.

[5] G.A.T. Sevilla, M.M. Hussain, Printed organic and inorganic electronics: devices to systems, IEEE J. Emerging on Selected Topics in Circuits and Systems 1 (2017) 147–160.
[6] G. Cummins, M.P.Y. Desmulliez, Inkjet printing of conductive materials: a review, Circ. World 38 (2012) 193–213.
[7] Z. Zhan, J. An, Y. Wei, V.T. Tran, H. Du, Inkjet-printed optoelectronics, Nanoscale 9 (2017) 965–993.
[8] D. Cherian, K.Y. Mitra, M. Hartwig, P.E. Malinowski, R.R. Baumann, Fabrication of organic photo detectors using inkjet technology and its comparison to conventional deposition processes, IEEE Sensors J 18 (2018) 94–105.
[9] A. Moya, G. Gabriel, R. Villa, F.J. del Campo, Inkjet-printed electrochemical sensors, Cur. Opin. Electrochem 3 (2017) 29–39.
[10] A. Salim, S. Lim, Review of recent inkjet-printed capacitive tactile sensors, Sensors 17 (2017), 2593 (1-20).
[11] Y. Zhang, N. Anderson, S. Bland, S. Nutt, G. Jursich, S. Joshi, All-printed strain sensors: building blocks of the aircraft structural health monitoring system, Sensor. Actuator. 253 (2017) 165–172.
[12] M. Orrill, S. LeBlanc, Printed thermoelectric materials and devices: fabrication techniques, advantages and challenges, J. Appl. Polym. Sci. 134 (2017), 44256 (1-15).
[13] S.S. Delekta, A.D. Smith, J. Li, M. Östling, Inkjet printed highly transparent and flexible graphene micro-supercapacitors, Nanoscale 9 (2017) 6998–7005.
[14] C.A. Milroy, S. Jang, T. Fujimori, A. Dodabalapur, A. Manthiram, Inkjet-printed lithium–sulfur microcathodes for all-printed, integrated nanomanufacturing, Small 13 (2017), 1603786 (1-11).
[15] H. Ji, D. Liu, H. Cheng, C. Zhang, Inkjet printing of vanadium dioxide nanoparticles for smart windows, J. Mater. Chem. C (2018), https://doi.org/10.1039/C8TC00286J.
[16] B. Derby, Inkjet printing ceramics: from drops to solid, J. Euro. Ceram. Soc. 31 (2011) 2543–2550.
[17] T.M. Eggenhuisen, Y. Galagan, A.F.K.V. Biezemans, T.M.W.L. Slaats, W.P. Voorthuijzen, S. Kommeren, S. Shanmugam, J.P. Teunissen, A. Hadipour, W.J.H. Verhees, S.C. Veenstra, M.J.J. Coenen, J. Gilot, R. Andriessen, W.A. Groen, High efficiency, fully inkjet printed organic solar cells with freedom of design, J. Mater. Chem. 3 (2015) 7255–7262.
[18] X. Peng, J. Yuan, S. Shen, M. Gao, A.S.R. Chesman, H. Yin, J. Cheng, Q. Zhang, D. Angmo, Perovskite and organic solar cells fabricated by inkjet printing: progress and prospects, Adv. Funct. Mater. 27 (2017), 1703704 (1-27).
[19] S. Sumaiya, K. Kardel, A. El-Shahat, Organic solar cell by inkjet printing - an overview, Technologies 5 (2017), 53 (1-18).
[20] X. Lin, J. Kavalakkatt, M. Ch. Lux-Steiner, A. Ennaoui, Inkjet-printed $Cu_2ZnSn(S,Se)_4$ solar cells, Adv. Sci. 2 (2015), 1500028–1000033.
[21] T. Martini, C. Chubilleau, O. Poncelet, A. Ricaud, A. Blayo, C. Martin, K. Tarasov, Spray and inkjet fabrication of Cu_2ZnSnS_4 thin films using nanoparticles derived from a continuous-flow microwave-assisted synthesis, Sol. Energy Mater. Sol. Cells 144 (2016) 657–663.
[22] L. Wang, X. Lin, A. Ennaoui, C. Wolf, M. Ch Lux-Steiner, R. Klenk, Solution-processed In_2S_3 buffer layer for chalcopyrite thin film solar cells, EPJ Photovolt 7 (2016) 70303–70307.
[23] X. Lin, R. Klenk, L. Wang, T. Köhler, J. Albert, S. Fiechter, A. Ennaoui, M. Ch Lux-Steiner, 11.3% efficiency $Cu(In,Ga)(S,Se)_2$ thin film solar cells via drop-on-demand inkjet printing, Energy Environ. Sci. 9 (2016) 2037–2043.
[24] R. Brisse, R. Faddoul, T. Bourgeteau, D. Tondelier, J. Leroy, S. Campidelli, T. Berthelot, B. Geffroy, B. Jousselme, Inkjet printing NiO-based p-type dye-sensitized solar cells, ACS Appl. Mater. Interfaces 9 (2017) 2369–2377.
[25] M. Colina, E. Bailo, B. Medina-Rodríguez, R. Kondrotas, Y. Sanchez-Gonzalez, D. Sylla, M. Placidi, M. Blanes, F. Ramos, A. Cirera, A.P. Rodríguez, E. Saucedo, Optimization of ink-jet printed precursors for $Cu_2ZnSn(S,Se)_4$ solar cells, J. Alloys Compd 735 (2018) 2462–2470.
[26] X. Lin, V.E. Madhavan, J. Kavalakkatt, V. Hinrichs, I. Lauermann, M. Ch Lux-Steiner, A. Ennaoui, R. Klenk, Inkjet-printed CZTSSe absorbers and influence of sodium on device performance, Sol. Energy Mater. Sol. Cells (2018), https://doi.org/10.1016/j.solmat.2017.09.003.
[27] T.K. Chaudhuri, D. Tiwari, Earth-abundant non-toxic Cu_2ZnSnS_4 thin films by direct liquid coating from metal–thiourea precursor solution, Sol. Energy Mater. Sol. Cells 101 (2012) 46–50.
[28] P.R. Ghediya, T.K. Chaudhuri, D. Vankhade, Electrical conduction of CZTS films in dark and under light from molecular solution ink, J. Alloys Compd 685 (2016) 498–506.
[29] F.H. Jardine, in: H.J. Emeleus, A.G. Sharpe (Eds.), Copper (I) Complexes, Advances in Inorganic Chemistry and Radiochemistry, vol 17, Academic Press, New York, 1975, pp. 115–163.
[30] M. Himmrich, H. Haeuseler, Far infrared studies on stannite and wurtzstannite type compounds, Spectrochim. Acta 47 (1991) 933–942.
[31] J. Tauc, A.J. Menth, States in the gap, J. Non-Cryst. Solids 8–10 (1972) 569–585.
[32] S. Chen, X.G. Gong, A. Walsh, S. Wei, Crystal and electronic band structure of Cu_2ZnSnX_4 (X=S and Se) photovoltaic absorbers: first-principles insights, Appl. Phys. Lett. 94 (2009) 041903–041905.
[33] V. Kosyak, M.A. Karmarkar, M.A. Scarpulla, Temperature dependent conductivity of polycrystalline Cu_2ZnSnS_4 thin films, Appl. Phys. Lett. 100 (2012) 263903–263907.
[34] M.Z. Ansari, N. Khare, Thermally activated band conduction and variable range hopping conduction in Cu_2ZnSnS_4 thin films, J. Appl. Phys. 117 (2015) 025706–025712.
[35] B.L. Guo, Y.H. Chen, X.J. Liu, W.C. Liu, A.D. Li, Optical and electrical properties study of sol-gel derived Cu_2ZnSnS_4 thin films for solar cells, AIP Adv. 4 (2014) 097115–097124.
[36] M. Hamdi, B. Louati, A. Lafond, C. Guillot-Deudon, B. Chrif, K. Khirouni, M. Gargouri, S. Jobic, F. Hlel, Structural and electrical properties of $Cu_2Zn(Sn_{1-x}Si_x)S_4$ ($x = 0$, $x = 0.5$) materials for photovoltaic applications, J. Alloys Compd 620 (2015) 434–441.
[37] P.R. Ghediya, T.K. Chaudhuri, J.R. Ray, Effect of light on hopping conduction in kesterite CZTS thin films, AIP Conf. Proc. 1728 (2016) 020020–020023.